Structural Modulations in the Intermediate Phase of Antiferroelectric PbHfO3

メタデータ	言語: eng 出版者: 公開日: 2019-08-30 キーワード (Ja): キーワード (En): 作成者: メールアドレス: 所属:
URL	https://doi.org/10.24517/00055243

This work is licensed under a Creative Commons Attribution-NonCommercial-ShareAlike 3.0 International License.

Structural Modulations in the Intermediate Phase of Antiferroelectric $PbHfO_3$

Hideshi Fujishita[1*], Kenichi Kato[2], Eiji Nishibori[3], Masaki Takata[2,4], Makoto Sakata[5], and Susumu Katano[6]

[1]*Institute of Liberal Arts and Science, Kanazawa University, Kanazawa 920-1192, Japan*

[2]*RIKEN SPring-8 Center, Sayo, Hyogo 679-5148, Japan*

[3]*Faculty of Pure and Applied Sciences, Tsukuba Research Center for Energy Materials Science, University of Tsukuba, Tsukuba, Ibaraki 305-8571, Japan*

[4]*Institute of Multidisciplinary Research for Advanced Materials (IMRAM), Tohoku University, Sendai 980-8577, Japan*

[5]*Japan Synchrotron Radiation Research Institute, SPring-8, Sayo, Hyogo 679-5198, Japan*

[6]*Graduate School of Science and Engineering, Saitama University, Saitama 338-8570, Japan*

We determine the crystal structure of the intermediate antiferroelectric (A_2) phase of $PbHfO_3$ by a Rietveld method using X-ray and neutron diffraction. The structure can be described by modulations associated with the lattice vibrational mode Σ_3(TO) with $\boldsymbol{q}$ = (0.15, 0.15, 0) and the R_{25}^{xy} mode, although the latter modulation is relatively distorted. The size of the orthorhombic unit cell is $\sqrt{2} \times 10\sqrt{2} \times 2$ times as large as that of the high-temperature cubic cell. The space group is Pbam-D_{2h}^9 (No. 55), and is the same as that of the room-temperature antiferroelectric (A_1) phase of $PbHfO_3$.

1. Introduction

Many ABO_3 perovskite oxides undergo phase transitions from the paraelectric (PE) state to the ferroelectric (FE), antiferroelectric (AFE), and other PE states on cooling. These transitions occur owing to the small energy differences among these states. Perovskite $PbZrO_3$ was the first AFE material to be discovered.[1–3] A D-E double-hysteresis loop is observed in the AFE phase, in contrast to the observation of the double-hysteresis loop in the PE phase of $BaTiO_3$. This is one of the pieces of direct evidence of the AFE property of $PbZrO_3$. The

*fujishit@staff.kanazawa-u.ac.jp

double-hysteresis loop of $PbZrO_3$ is observed owing to the forced transition from the AFE state to the FE state. The small energy difference between these states is overcome by the application of an external electric field. Applications of perovskite oxides in technology are possible owing to the small energy differences. The AFE perovskites have attracted much attention because of their applications in technology such as actuators, transducers, and FE random access memories, for example.[4)]

Another piece of direct evidence of the AFE property of $PbZrO_3$ is the antiparallel shifts of Pb atoms in the [110] direction of the high-temperature cubic perovskite cell.[5)] These shifts cause a superstructure with the unit cell of $4a_p \times 4a_p \times c_p$, where a_p and c_p are the lattice parameters of the pseudotetragonal perovskite sublattice. Cochran and Zia first pointed out that the structural modulation with the antiparallel shifts of Pb atoms is the modulation associated with the lattice vibrational mode Σ_3(TO) with the wave vector $\boldsymbol{q}$ = (1/4, 1/4, 0).[6)] We showed that structural modulations in the AFE phase are those associated with the lattice vibrational modes Σ_3(TO) and R_{25}^{xy},[7)] although the latter modulation is relatively distorted.[8,9)] The latter modulation causes a superstructure with the unit cell of $2a_p \times 2a_p \times 2c_p$. Then, the superstructure of the AFE $PbZrO_3$ has the unit cell of $4a_p \times 4a_p \times 2c_p$. The size of its crystallographically standard unit cell is $\sqrt{2}a_p \times 2\sqrt{2}a_p \times 2c_p$.

Perovskite $PbHfO_3$ undergoes two AFE phase transitions.[10,11)] The room-temperature AFE phase (A_1) of $PbHfO_3$ is isostructural with that of $PbZrO_3$.[12)] We showed that structural modulations in the A_1 phase are those associated with the lattice vibrational modes Σ_3(TO) with the wave vector $\boldsymbol{q}$ = (1/4, 1/4, 0) and R_{25}^{xy}, although the modulation associated with the R_{25}^{xy} mode is relatively distorted.[13)]

$PbHfO_3$ has an intermediate AFE phase (A_2).[10,11)] We have reported that AFE superlattice reflections with $\boldsymbol{q}$ = (1/4, 1/4, 0) disappear at 435 K, and reflections associated with a large cell volume appear between 435 and 480 K by heating in powder X-ray diffraction experiments of $PbHfO_3$.[14)] The reflections associated with R_{25}^{xy} remain in the A_2 phase. We suggested that the superstructure has a size of $5a_p \times 5a_p \times 8c_p$. Recently, the symmetry of the A_2 phase has been determined to be orthorhombic by X-ray diffraction and birefringence measurements.[15)] We can determine the crystal structure of the A_2 phase of $PbHfO_3$ by synchrotron radiation and neutron diffraction experiments in this work. The details of the study are reported herein. The unit cell size of the superstructure is revised on the basis of our results.

2. Experimental details

2.1 Synthesis

Ceramic samples were obtained by a solid-state reaction of PbO and HfO_2. The purity of PbO was 99.999% (Rare Metallic), and that of HfO_2 was 99.95% (Rare Metallic). A mixture of PbO and HfO_2 was successively fired at 600, 800, and 1000 °C, and subsequently at 1150 °C for 10 h with intermediate grinding.

2.2 X-ray diffraction data collection

An X-ray diffraction pattern was collected at 460 K using synchrotron radiation. The experiment was performed using a large Debye-Scherrer camera with a radius of 286.5 mm installed at the BL02B2 beam line in SPring-8.[16] It uses an imaging-plate system as a detector. The intensity data were collected at steps of 0.01° (2θ) from the imaging plate. The wavelength of the incident beam was 0.5 Å. The powder sample was sealed into a quartz capillary of 0.1 mm internal diameter and 0.01 mm thickness. The absence of the preferred orientation effect was ascertained by the uniform intensity along each Debye ring. The sample was heated by a hot air flow. The temperature was controlled to within 1 K.

2.3 Neutron diffraction data collection

A powder neutron diffraction pattern was obtained at 460 K using a high-resolution powder diffractometer (HRPD) installed at JRR-3M in JAERI. This diffractometer consists of 64 detectors, and the angle between the detectors is 2.5°. The incident neutron wavelength was 1.8232 Å. The collimation was 40'-20'-6'. The powder specimen obtained by grinding the ceramic samples was placed in an electric furnace. The temperature was controlled to within 1 K. A vanadium sample cell of 10 mm diameter was used to avoid diffraction peaks from the cell. The intensity data were collected by scanning using a counter system with 0.05° steps (2θ) over an angle of 2.5°.

2.4 Analysis

The obtained diffraction patterns were analyzed by the Rietveld method using the computer program RIETAN-FP.[17] The background level was fitted using a polynomial expression throughout the analysis. A pseudo-Voigt function was applied to the profile of the diffraction peaks. A conjugate direction method was employed in the least-squares refinements.

We analyzed the obtained X-ray diffraction pattern between 2θ = 5.8° and 75.3°. A relatively strong background peak exists at 7°, which is caused by the quartz capillary. The peak was difficult to express using the polynomial background function. Subsequently, the back-

ground level where no diffraction peaks appear below 9° was replaced by the calculated background. The replaced areas were excluded in the refinement calculations. The background level below 11° where peaks appear was drawn to connect the replaced areas smoothly by linear functions.

The sample contained heavy Pb atoms and Hf atoms. Subsequently, the absorption was corrected in the analysis of the X-ray diffraction pattern. We used 0.6 for the value of μr because of the reason stated previously for the same sample.[18] The absorption was also corrected in the analysis of the neutron diffraction pattern, because the absorption of neutrons by Hf atoms is large (102×10^{-24} cm^2 for neutrons with a wavelength of 1.8 Å). A packing ratio of 0.41 was used for the correction. This value was calculated using the weight and volume of our sample. The volume was measured using a graduated cylinder.

3. Results

A low-angle part of the X-ray diffraction pattern in the intermediate AFE phase (A_2) of $PbHfO_3$ measured at 460 K is delineated by a red line in the upper portion of Fig. 1. The X-ray diffraction pattern in the A_1 phase of $PbHfO_3$ at 400 K is drawn by a blue line in the lower portion for comparison; we reported this pattern previously.[18] All the diffraction peaks could be successfully indexed as shown in the figure, where the indices are based on a pseudotetragonal perovskite cell; $q_I = 0.15$ and $q_A = 0.25$. Furthermore, R_{25} indicates the peak caused by a structural modulation associated with the R_{25} lattice vibrational mode.

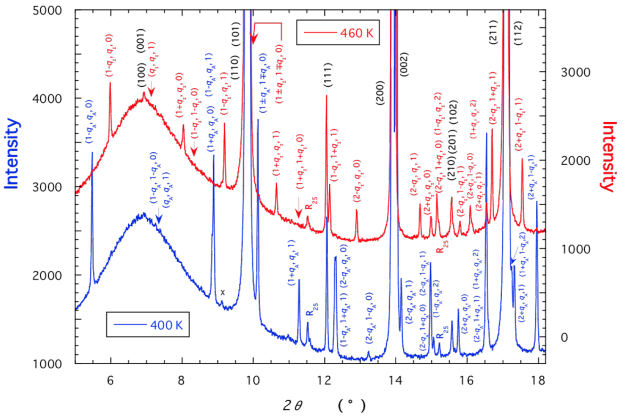

Fig. 1. (Color online) Low-angle X-ray diffraction patterns of $PbHfO_3$ measured at 460 K (A_2 phase; red line in the upper portion) and 400 K (A_1 phase; blue line in the lower portion). The X-ray wavelength is 0.5 Å. Indices are assigned on the basis of a pseudotetragonal perovskite cell, where $q_I = 0.15$ and $q_A = 0.25$. R_{25} is a reflection caused by a structural modulation associated with the lattice vibrational mode R_{25}. Indices of unobserved reflections are also shown. An impurity peak is indicated by "x".

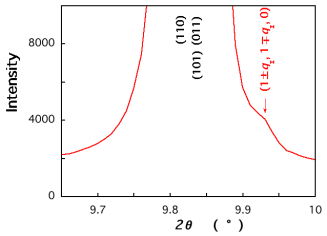

Fig. 2. (Color online) Enlarged X-ray diffraction pattern around (110) reflection of $PbHfO_3$ at 460 K to show the appearance of superlattice reflection $(1\pm q_I, 1\mp q_I, 0)$, where $q_I = 0.15$.

Superlattice reflections with the indices $(1\pm q_I, 1\pm q_I, 0)$ disappear around the strongest fundamental (110) reflection, where the compounds are in the same order. However, reflections with $(1\pm q_I, 1\mp q_I, 0)$ appear, although they are close to the fundamental reflection and we can only confirm their existence as a "shoulder" at the hem of the fundamental reflection, as shown in Fig. 2. These facts indicate that the structural modulation has a character of a transverse mode with the wave vector $\boldsymbol{q}$ = (0.15, 0.15, 0) polarized in the (001) plane. The superlattice-reflection intensities around the very weak (100) reflection have the same order as those around (110): they have no simple relation with the intensity of the fundamental reflection. This fact indicates that the modulation has a character of an optical mode. Typically, a lattice vibrational Σ_3(TO) branch traveling in the [110] direction is the lowest-energy branch in optical branches along [110] in perovskite compounds. In fact, the modulation in the A_1 phase of $PbHfO_3$ is associated with the Σ_3(TO) mode with $\boldsymbol{q}$ = (1/4, 1/4, 0). The modulation associated with the Σ_3(TO) mode with $\boldsymbol{q}$ = (0.15, 0.15, 0) causes a superstructure with the unit cell size of $20a_p \times 20a_p \times c_p$, where a_p and c_p are the lattice parameters of the pseudotetragonal perovskite sublattice.

Superlattice reflections with indices $(h \pm 1/2, k \pm 1/2, l \pm 1/2)$ are caused by the modulation associated with the R_{25}^{xy} mode, where h, k, and l are integers. This modulation consists of those associated with the R_{25}^{x} and R_{25}^{y} modes: the former is antidirectional rotations of oxygen octahedra around [100] in the adjacent perovskite cell, while the latter is those around [010]. Both the amplitudes are equal and defined as A_R. The modulations cause the superstructure with the unit cell of $2a_p \times 2a_p \times 2c_p$. Then, the superstructure of the A_2 phase has the unit cell of $20a_p \times 20a_p \times 2c_p$. Its crystallographically standard orthorhombic unit cell has a size of $\sqrt{2}a_p \times 10\sqrt{2}a_p \times 2c_p$. There are three wavelengths of the Σ_3(TO)-type modulation in the length of $10\sqrt{2}a_p$ along [110] in the perovskite cell.

Referring to Cowley's table,[19] the atomic displacements in the A_2 phase of $PbHfO_3$ asso-

ciated with the Σ_3(TO) with $\boldsymbol{q}$ = (0.15, 0.15, 0) and R_{25}^{xy} modes can be concluded, as schematically shown in Fig. 3, if we ignore the distortions in the modulations. The space group is Pbam-D_{2h}^{9} (No. 55), which is the same as that of the A_1 phase. The atomic positions associated with these modes are summarized in Appendix. In Cowley's table, oxygen atoms of the cubic perovskite structure are labeled as OI, OII, and OIII, and their positions are (1/2, 1/2, 0), (1/2, 0, 1/2), and (0, 1/2, 1/2), respectively. Moreover, the positions of Pb and Hf atoms are (0, 0, 0) and (1/2, 1/2, 1/2), respectively.

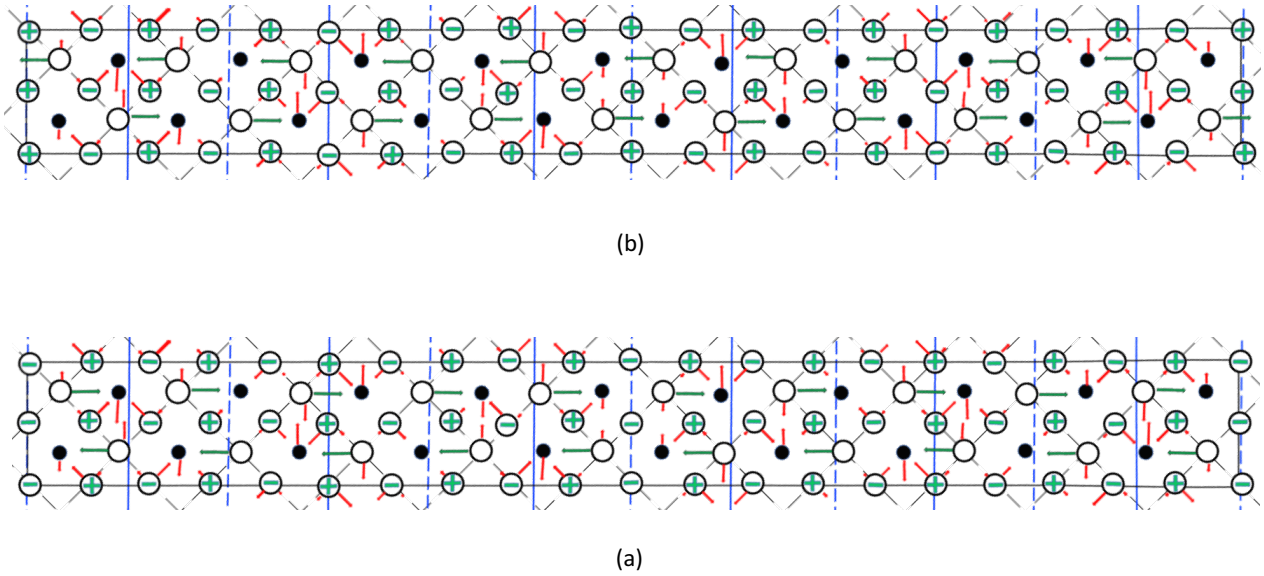

Fig. 3. (Color online) Schematic projections of undistorted atomic displacements associated with modes with Σ_3(TO) with $\boldsymbol{q}$ = (0.15, 0.15, 0) and R_{25}^{xy} onto the ab plane of $PbHfO_3$ in the intermediate (A_2) phase. The solid circles and open circles indicate Pb atoms and oxygen atoms, respectively. (a) shows the atoms in the planes $z = 0$ and $z = c_p/2$, while (b) shows the atoms in the planes $z = c_p$ and $z = 3c_p/2$, where c_p is the pseudotetragonal lattice parameter of the perovskite sublattice in the z-direction. The perovskite sublattices in the ab plane are delineated by dashed black lines. The solid black lines delineate the orthorhombic cell. The dashed and solid blue lines indicate the nodes and antinodes of modulation with $\boldsymbol{q}$, respectively. The arrows and + or - signs denote the directions of the displacement of atoms from the cubic perovskite sites. The red arrows and green arrows or signs denote the directions associated with Σ_3(TO) and R_{25}^{xy}, respectively. The lengths of arrows are drawn on the basis of the amplitudes of modulations obtained by the analysis of X-ray and neutron diffraction patterns, but are exaggerated. Hf atoms are omitted on the basis of the analysis.

The X-ray and neutron diffraction patterns in the A_2 phase were analyzed by the Rietveld method on the basis of this structure model. Selected structural parameters of Pb and Hf atoms were refined by the X-ray diffraction pattern. Other parameters were subordinated to

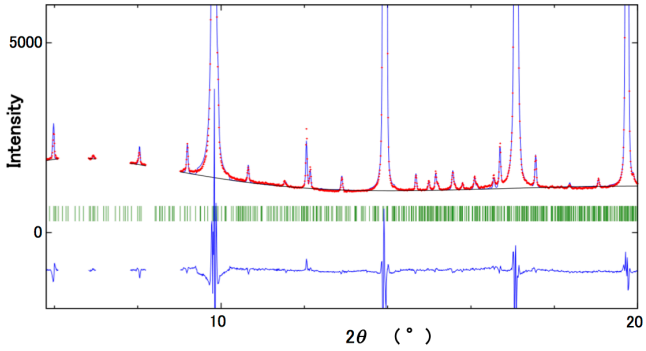

Fig. 4. (Color online) X-ray Rietveld refinement pattern of $PbHfO_3$ at 460 K (A_2 phase). Only the low-angle and small-intensity part of the pattern is displayed. The X-ray wavelength is 0.5 Å. The calculated pattern is denoted by the blue line passing through the red data points in the upper portion. The calculated background level is indicated by the black line. The difference between the observed and calculated patterns is shown by the blue line in the lower portion. The short green bars indicate the positions of possible reflections. The refinement was performed using six selected fractional coordinates of atoms and three thermal parameters for three elements (see text).

these parameters. Subsequently, selected structural parameters of oxygen atoms were refined by the neutron diffraction pattern. This procedure was repeated several times until converged results were obtained. The R-factors R_{wp} were 3.05 and 6.81% for the X-ray and neutron diffraction, respectively. The result of profile fitting to the observed X-ray diffraction pattern is shown in Fig. 4, where only the small-intensity part at the low angle is indicated to show the fitting to superlattice reflections well. The obtained parameters were x(Pb1)=0.7671(1), B_{Pb}=2.84 (2) Å^2, x(Hf1)=0.2521(1), B_{Hf}=0.56 (1) Å^2, x(O1)=0.2358(7), y(O1)=0.02948(3), x(O8)=-0.0204(9), y(O8)=0.04877(8), B_O=1.73 (5) Å^2, where the same values of thermal parameters were assumed for atoms of the same element. These coordinates mean that the amplitudes of the modulations in Appendix are A_{Pb}=0.220 (2) Å, A_{Hf}=0.027 (2) Å, A_{OI}=-0.186 (9) Å, A_{OII}=0.042 (10) Å, A_{OIII}=0.168(10) Å, and A_R=0.185 (3) Å. The value of A_R corresponds to the 7.3 (2)° rotation of the oxygen octahedra around [110].

Finally, we refined all crystallographically independent parameters. The positions of the Pb and Hf atoms were refined by the X-ray diffraction pattern, and the oxygen positions were refined by the neutron diffraction pattern. This procedure was repeated several times until converged results were obtained. The R-factors R_{wp} were 2.97 and 5.92% for the X-ray and neutron diffraction, respectively. The result of profile fitting to the X-ray diffraction pattern is shown in Fig. 5. The orthorhombic lattice parameters are a = 5.850(3) Å, b = 58.50(3) Å, and c = 8.235(3) Å. The result of profile fitting to the neutron diffraction pattern is shown in Fig. 6. The obtained structural parameters are listed in Table I.

Table I. Structural parameters (fractional coordinates and thermal parameters) of $PbHfO_3$ obtained by X-ray and neutron diffraction in intermediate antiferroelectric (A_2) phase. The space group Pbam-D^9_{2h} (No. 55) was used. Isotropic thermal parameters were used for all atoms. The numbers in parentheses indicate the estimated standard deviations. The lattice parameters are a = 5.850(3) Å, b = 58.50(3) Å, and c = 8.235(3) Å.

Atom	Site	x	y	z	B (Å^2)
Pb1	4g	0.779(4)	0.0261(4)	0.0	2.68(2)
Pb2	4g	0.282(3)	0.0756(4)	0.0	2.68
Pb3	4g	0.782(4)	0.1253(3)	0.0	2.68
Pb4	4g	0.220(4)	0.1764(4)	0.0	2.68
Pb5	4g	0.714(4)	0.2250(4)	0.0	2.68
Pb6	4h	0.768(4)	0.0257(4)	0.5	2.68
Pb7	4h	0.284(3)	0.0755(4)	0.5	2.68
Pb8	4h	0.770(3)	0.1266(3)	0.5	2.68
Pb9	4h	0.244(4)	0.1742(4)	0.5	2.68
Pb10	4h	0.721(4)	0.2255(4)	0.5	2.68
Hf1	8i	0.254(3)	0.0246(3)	0.2483(14)	0.51(2)
Hf2	8i	0.7564(14)	0.0749(3)	0.2566(12)	0.51
Hf3	8i	0.2590(19)	0.12534(15)	0.2482(16)	0.51
Hf4	8i	0.752(3)	0.1751(3)	0.2474(13)	0.51
Hf5	8i	0.2528(16)	0.2247(3)	0.2466(14)	0.51
O1	4g	0.311(8)	0.0269(7)	0.0	0.98(6)
O2	4g	0.740(7)	0.0699(7)	0.0	0.98
O3	4g	0.224(8)	0.1267(7)	0.0	0.98
O4	4g	0.759(7)	0.1694(7)	0.0	0.98
O5	4g	0.280(7)	0.2246(7)	0.0	0.98
O6	4e	0.0	0.0	0.205(5)	0.98
O7	4f	0.5	0.0	0.223(5)	0.98
O8	8i	-0.020(6)	0.0478(5)	0.304(3)	0.98
O9	8i	0.515(5)	0.0467(5)	0.293(3)	0.98
O10	8i	-0.044(5)	0.1038(5)	0.240(4)	0.98
O11	8i	0.471(5)	0.0983(5)	0.250(4)	0.98
O12	8i	-0.005(6)	0.1505(5)	0.270(3)	0.98
O13	8i	0.471(5)	0.1524(5)	0.267(3)	0.98
O14	8i	-0.006(5)	0.2007(5)	0.249(3)	0.98
O15	8i	0.492(5)	0.1991(5)	0.211(3)	0.98
O16	8i	0.002(5)	0.2508(4)	0.263(3)	0.98
O17	4h	0.211(8)	0.0196(8)	0.5	0.98
O18	4h	0.712(7)	0.0815(7)	0.5	0.98
O19	4h	0.234(8)	0.1215(7)	0.5	0.98
O20	4h	0.737(8)	0.1824(7)	0.5	0.98
O21	4h	0.290(7)	0.2209(7)	0.5	0.98

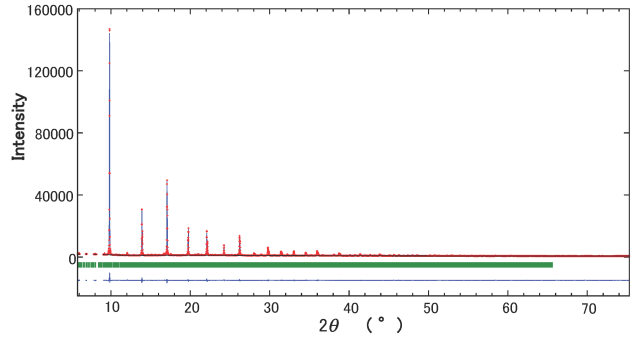

Fig. 5. (Color online) X-ray Rietveld refinement pattern of $PbHfO_3$ at 460 K (A_2 phase) obtained using all possible parameters for Pb and Hf atoms. The X-ray wavelength is 0.5 Å. Only the positions of 15000 possible reflections with $2\theta < 66°$ are indicated by short green bars.

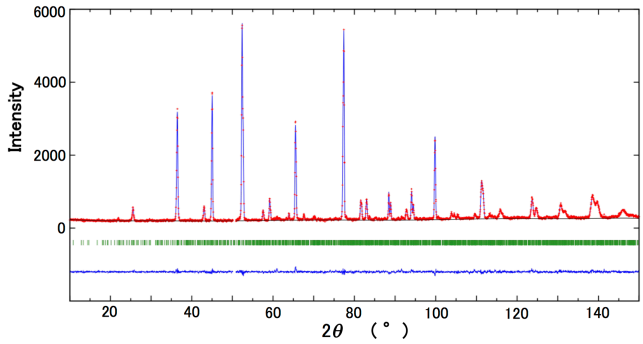

Fig. 6. (Color online) Neutron Rietveld refinement pattern of $PbHfO_3$ at 460 K (A_2 phase) obtained using all possible parameters for oxygen atoms. The neutron wavelength is 1.8232 Å.

4. Discussion

The X-ray and neutron powder diffraction patterns of $PbHfO_3$ in the A_2 phase could be fitted well by the structural modulations associated with the lattice vibrational mode Σ_3(TO) with $\boldsymbol{q}$ = (0.15, 0.15, 0) and the R_{25}^{xy} mode. The fitting to the X-ray diffraction pattern was not improved significantly using all the crystallographically independent parameters for Pb and Hf atoms. This result indicates that structural modulations for Pb and Hf atoms associated with the Σ_3(TO) mode are not distorted significantly. In fact, no meaningful displacements of Hf atoms could be detected from the pseudotetragonal perovskite positions. No meaningful displacements of Pb atoms could be detected along the *b*-direction as well. In addition, no meaningful differences could be detected between the displacements along the *a*-direction for Pb atoms with z = 0 and 0.5, although the errors are relatively large.

The fitting to the neutron diffraction pattern was improved using all the crystallographically independent parameters for the oxygen atoms. This result indicates that the structural

modulation associated with the R_{25}^{xy} mode is relatively distorted. In fact, meaningful distortions of oxygen displacements are observed along the *c*-direction.

Two independent lattice vibrational modes, Σ_3(TO) with $\boldsymbol{q}$ = (0.15, 0.15, 0) and R_{25}^{xy}, cause the PE to AFE A_2 phase transition. The successive transition to the AFE A_1 phase is caused by the lattice vibrational mode Σ_3(TO) with $\boldsymbol{q}$ = (1/4, 1/4, 0), which has the same symmetry as the Σ_3(TO) mode with $\boldsymbol{q}$ = (0.15, 0.15, 0), thus extricating the modulation associated with the Σ_3(TO) mode with $\boldsymbol{q}$ = (0.15, 0.15, 0). Such mechanisms are expected to create first-order transitions. In fact, the dielectric constant[10,11] and specific heat[20] measurements have shown the first-order nature of the successive phase transitions.

The dielectric constant of $PbHfO_3$ becomes large at the PE to A_2 phase transition in the PE phase. This means that the FE Γ_{15} mode becomes soft, which is the Σ_3(TO) mode with $\boldsymbol{q}$ = 0. Subsequently, the energy of the Σ_3(TO) branch along [110] is expected to be low from $\boldsymbol{q}$ = 0 to (1/4, 1/4, 0) in the PE phase. The detection of this softening is desirable.

5. Conclusions

The crystal structure of the intermediate AFE (A_2) phase of $PbHfO_3$ was analyzed by X-ray and neutron powder diffraction experiments. The structure could be described by the structural modulations associated with the lattice vibrational mode Σ_3(TO) with $\boldsymbol{q}$ = (0.15, 0.15, 0) and the R_{25}^{xy} mode. The size of the orthorhombic unit cell was $\sqrt{2} \times 10 \sqrt{2} \times 2$ times as large as that of the high-temperature cubic cell. The space group was Pbam-D_{2h}^9 (No. 55), and was the same as that of the room-temperature AFE (A_1) phase.

Acknowledgments

The synchrotron radiation experiments were performed at BL02B2 in SPring-8 with the approval of the Japan Synchrotron Radiation Research Institute (JASRI) (Proposal No. 2001A0192-ND-np).

References

1) E. Sawaguchi, G. Shirane, and Y. Takagi, J. Phys. Soc. Jpn. **6**, 333 (1951).

2) G. Shirane, E. Sawaguchi, and Y. Takagi, Phys. Rev. **84**, 476 (1951).

3) E. Sawaguchi and T. Kittaka, J. Phys. Soc. Jpn. **7**, 336 (1952).

4) J. F. Scott, Science **315**, 954 (2007).

5) E. Sawaguchi, H. Maniwa, and S. Hoshino, Phys. Rev. **83**, 1078 (1951).

6) W. Cochran and A. Zia, Phys. Status Solidi **25**, 273 (1968).

7) H. Fujishita and S. Hoshino, J. Phys. Soc. Jpn. **53**, 226 (1984).

8) H. Fujishita and S. Katano, J. Phys. Soc. Jpn. **66**, 3484 (1997).

9) H. Fujishita, Y. Ishikawa, S. Tanaka, A. Ogawaguchi, and S. Katano, J. Phys. Soc. Jpn. **72**, 1426 (2003).

10) G. Shirane and R. Pepinsky, Phys. Rev. **91**, 812 (1953).

11) G. A. Samara, Phys. Rev. B **1**, 3777 (1970).

12) D. L. Corker, A. M. Glazer, W. Kaminsky, R. W. Whatmore, J. Dec, and K. Roleder, Acta Crystallogr., Sect. B **54**, 18 (1998).

13) H. Fujishita, A. Ogawaguchi, and S. Katano, J. Phys. Soc. Jpn. **77**, 064601 (2008).

14) H. Fujishita and Y. Ishikawa, Ferroelectrics **269**, 135 (2002).

15) S. Huband, A. M. Glazer, K. Roleder, A. Majchrowski, and P. A. Thomas, J. Appl. Crystallogr. **50**, 378 (2017).

16) E. Nishibori, M. Takata, K. Kato, M. Sakata, Y. Kubota, S. Aoyagi, Y. Kuroiwa, M. Yamakata, and N. Ikeda, Nucl. Instrum. Methods Phys. Res., Sect. A **467-468**, 1045 (2001).

17) F. Izumi and K. Momma, Solid State Phenom. **130**, 15 (2007).

18) H. Fujishita, Y. Ishikawa, A. Ogawaguchi, K. Kato, E. Nishibori, M. Takata, and M. Sakata, J. Phys. Soc. Jpn. **74**, 2743 (2005).

19) R. A. Cowley, Phys. Rev. **134**, A981 (1964).

20) M. Maczka, T. H. Kim, A. Gagor, I. Jankowska-Sumara, A. Majchrowski, and S. Kojima, J. Alloys Compd. **622**, 935 (2015).

Appendix: Numbers of equivalent positions, Wyckoff notations, and fractional coordinates of atoms

The number of equivalent positions and Wyckoff notation of each atom are written in parentheses immediately after the name of the atom. The fractional coordinates (x, y, z) of the atom from the undistorted structural modulations associated with the Σ_3(TO) mode with $\boldsymbol{q}$ = (0.15, 0.15, 0) and R_{25}^{xy} are written in the next parentheses. The space group is Pbam-D_{2h}^{9} (No. 55). a_p and c_p are lattice parameters of the pseudotetragonal perovskite sublattice. A_{Pb}, A_{Hf}, A_{OI}, A_{OII}, and A_{OIII} are the amplitudes of the structural modulations associated with the Σ_3(TO) mode. A_R is the amplitude of the oxygen atoms associated with R_{25}^{x} and R_{25}^{y}.

Pbn (n=1 – 5) (4g) $(0.25 \times (2n+1) + A_{Pb} sin(6\pi \times 0.025 \times (2n-1))/\sqrt{2}a_p, 0.025 \times (2n-1), 0.0)$

Pbn (n=6 – 10) (4h) $(0.25 \times (2n-9) + A_{Pb} sin(6\pi \times 0.025 \times (2n-11))/\sqrt{2}a_p, 0.025 \times (2n-11), 0.5)$

Hfn (n=1 – 5) (8i) $(0.25 \times (2n-1) + A_{Hf} sin(6\pi \times 0.025 \times (2n-1))/\sqrt{2}a_p, 0.025 \times (2n-1), 0.25)$

On (n=1 – 5) (4g) $(0.25 \times (2n-1) + A_{OI} sin(6\pi \times 0.025 \times (2n-1))/\sqrt{2}a_p, 0.025 \times (2n-1) + (-1)^{n+1} \times A_R/10a_p, 0.0)$

On (n=6, 7) (4e/4f) $(0.0, 0.5 \times (n-6), 0.25 - A_R/2c_p)$

On (n=8,12,16) (8i) $(0.5 \times (n-6) - (A_{OII} + A_{OIII}) sin(6\pi \times 0.025 \times (n-6))/2a_p,$
$0.025 \times (n-6) + (A_{OII} - A_{OIII}) sin(6\pi \times 0.025 \times (n-6))/20a_p, 0.25 + A_R/2c_p)$

On (n=9,13) (8i) $(0.5 \times (n-6) - (A_{OII} + A_{OIII}) sin(6\pi \times 0.025 \times (n-6))/2a_p,$
$0.025 \times (n-7) - (A_{OII} - A_{OIII}) sin(6\pi \times 0.025 \times (n-7))/20a_p, 0.25 + A_R/2c_p)$

On (n=10,14) (8i) $(0.5 \times (n-6) - (A_{OII} + A_{OIII}) sin(6\pi \times 0.025 \times (n-6))/2a_p,$
$0.025 \times (n-6) - (A_{OII} - A_{OIII}) sin(6\pi \times 0.025 \times (n-6))/20a_p, 0.25 - A_R/2c_p)$

On (n=11,15) (8i) $(0.5 \times (n-6) - (A_{OII} + A_{OIII}) sin(6\pi \times 0.025 \times (n-7))/2a_p,$
$0.025 \times (n-7) + (A_{OII} - A_{OIII}) sin(6\pi \times 0.025 \times (n-7))/20a_p, 0.25 - A_R/2c_p)$

On (n=17 – 21) (4h) $(0.25 \times (2n-33) + A_{OI} sin(6\pi \times 0.025 \times (2n-33))/\sqrt{2}a_p, 0.025 \times (2n-33) + (-1)^{n-16} \times A_R/10a_p, 0.5)$